DOI: 10.1002/((please add manuscript number))
Article type: Communication

Controllable, Wide-Ranging n- and p-Doping of Monolayer Group 6 Transition-metal Disulfides and Diselenides

Siyuan Zhang, Heather M. Hill, Karttikay Moudgil, Curt A. Richter, Angela R. Hight Walker, Stephen Barlow, Seth R. Marder, Christina A. Hacker,* Sujitra J. Pookpanratana**

Dr. S. Zhang
Theiss Research, La Jolla, CA 92037, USA
E-mail: siyuan.zhang@nist.gov

Dr. S. Zhang, Dr. H. M. Hill, Dr. C. A. Richter, Dr. A. R. Hight Walker, Dr. C. A. Hacker, Dr. S. J. Pookpanratana
Physical Measurement Laboratory, National Institute of Standards and Technology (NIST)
Gaithersburg, MD 20899, USA
E-mail: christina.hacker@nist.gov; sujitra@nist.gov

Dr. K. Moudgil, Dr. S. Barlow, Prof. S. R. Marder
Center for Organic Photonics and Electronics, and School of Chemistry and Biochemistry
Georgia Institute of Technology
Atlanta, GA 30332, USA

Keywords: transition metal dichalcogenides, electron-transfer doping, field-effect transistors, photoluminescence, redox-active molecules

Abstract

Developing processes to controllably dope transition-metal dichalcogenides (TMDs) is critical to achieving commercially viability for optical and electrical applications. In this study, molecular reductants and oxidants are introduced onto a series of monolayer TMDs, specifically MoS_2, WS_2, $MoSe_2$, and WSe_2. Doping was achieved by exposing the TMD surface to solutions of pentamethylrhodocene dimer as the molecular reductant (n-dopant) and "Magic Blue," $[N(C_6H_4\text{-}p\text{-}Br)_3]SbCl_6$, as the molecular oxidant (p-dopant). Current-voltage characteristics of TMD-based field-effect transistors show that, regardless of their initial transport behavior, all four TMDs can be used in either p- or n-channel devices when appropriately doped. The extent of doping can be conveniently controlled by varying the concentration of dopant solutions and treatment time, and, in some cases, both non-degenerate and degenerate regimes are accessible.

Photoluminescence (PL) properties of the doped monolayer TMDs were measured; for all four materials the PL intensity is enhanced with p-doping but reduced with n-doping. Raman and X-ray photoelectron spectroscopies (XPS) also provide insight into the underlying physical mechanism by which the molecular reductants and oxidants react with the monolayer. Estimates of changes of carrier density from electrical, PL, and XPS results were compared. Overall a simple and effective route to tailor the electrical and optical properties of TMDs is demonstrated.

Layered transition-metal dichalcogenides (TMDs) are an emerging class of two-dimensional materials with unique thickness-dependent optical and electrical properties.[1] Analogous to graphene, but with a wide range of band gaps, mono- and few-layer TMDs are both fundamentally and technologically intriguing, and have been considered as promising candidates for next-generation electronic and optoelectronic devices. Molybdenum and tungsten dichalcogenides, MX_2 (M = Mo or W, X = S or Se), in particular, have tunable bandgaps and strong absorption of incident solar illumination at atomic thickness, which make them very attractive for optoelectronics applications.[2] For low-power, high-performance complementary logic applications, both n- and p-type field effect transistors (FETs) must be developed. The ultrathin nature and large surface area of 2D materials make them quite sensitive to their surrounding environments, which enables charge transport to be tuned through post-modification. Many studies have focused on modulating the carrier type and density in a controllable manner.[3] Adapting ideas from Si-based semiconductor technology, several approaches have been reported, including synthesis of mixed-chalcogen TMD alloys,[4] substitutional doping with other elements that contribute a different number of valence electrons (e.g., replacing Mo by Re, Nb, or Zr),[5] thermal diffusion or implantation of foreign atoms,[6] and plasma etching.[7] However, unwanted side-effects may generate defects in the crystalline lattice of the sub-nanometer thick films.[3] The physi- or chemisorption of gases has also been reported. NO_x, H_2O, and O_2 are found to be p-doping species because of their oxidizing

characteristics.[8] The physisorbed gas molecules can be easily desorbed in ambient conditions after a short time, while the chemisorbed gases perturb the original band structure of TMDs and alter the semiconducting transport to metallic.[8] An alternate route to modulate the electronic properties of TMDs is to use surface modification with partial or full electron charge transfer. Organic modifiers have been used to induce partial charge transfer and/or surface dipoles on the host material. For example, Lewis basic organics, such as NH_2-containing species, have been used as n-dopants,[9] while acids, halogens, and metal halides have been widely used as p-dopants.[10] Another approach is the use of redox-active molecules that can undergo integral electron-transfer reactions with the TMD,[11] and potentially produce stronger and nondestructive doping effects compared with the previously mentioned methods.

Recently, we demonstrated effective doping of trilayer wafer-scale MoS_2 and WSe_2,[11b, 11c] using molecular reductants and oxidants. The molecular reductants and oxidants are introduced onto the surface of 2D materials from solution. Effective modulation of the carrier concentration and significant shifts of the work-function were observed. However, neither p-type transport behavior of MoS_2 nor n-type behavior of WSe_2 could be observed, even at high dopant concentration and longer treatment time; this may be attributable to the large number of defect states of the as-grown TMD layers and/or to the effects of Fermi level pinning at the metal–TMD interface. In this study, we successfully expand the application of electron-transfer doping using molecular reductants and oxidants to monolayer TMDs – specifically to monolayer MoS_2, $MoSe_2$, WS_2, and WSe_2 – transferred through gold-mediated exfoliation[12] to ensure relatively high-quality and low-defect density films. We demonstrate a wide-range of controllable n- and p-doping by choice of molecular reductant or oxidant for all four MX_2 materials. Both n- and p-type transport properties are observed in all four monolayer-TMDs through doping, and the degree of doping is controllable through the choice of dopants, treatment time, and the concentration of doping solution. The ability to achieve both n- and p-type transport on the

same material can facilitate the fabrication of inverters and junctions, e.g., p-n junctions for diodes and p-n-p junctions for FETs. The doping process is investigated in detail through electrical measurements, photoluminescence (PL), Raman, and X-ray photoelectron spectroscopic (XPS) measurements.

The four TMD monolayers were transferred according to the gold-mediated exfoliation method reported by Desai *et al.*[12] onto a Si/SiO_2 substrate with a 300 nm oxide layer. Monolayer TMDs were regularly obtained with average areas between 50 μm^2 and 100 μm^2 (Figure S1-S2). Here, pentamethylrhodocene dimer, $(RhCp^*Cp)_2$,[13] was used as the molecular reductant (n-dopant) and tris(4-bromophenyl)ammoniumyl hexachloroantimonate ("Magic Blue," MB, $[N(C_6H_4\text{-}p\text{-}Br)_3]SbCl_6$),[14] as the molecular oxidant (p-dopant), and their chemical structures are shown in **Figure 1**a. Figure 1b shows the valence band maxima (E_v) and conduction band minima (E_c) obtained from previously reported density functional theory (DFT) calculations for monolayer TMDs.[15] Both valence and conduction band energies increase (i.e., move towards the vacuum level) in the order $MoS_2 < WS_2 < MoSe_2 < WSe_2$. Figure 1b also shows estimates of relevant energy levels for the dopants used. MB is a strong p-dopant, the cation of which is reduced at a potential of +0.70 V vs. ferrocene $(FeCp_2)^{+/0}$,[16] from which an electron affinity (EA) of ca. 5.5 eV can be estimated.[17] The n-dopant used in this study, $(RhCp^*Cp)_2$, reacts via coupled bond-cleavage/electron-transfer pathways to form two monomeric cations, $RhCp^*Cp^+$ (Figure 1c), and releases two electrons. The effective $RhCp^*Cp^+ /0.5(RhCp^*Cp)_2$ redox potential is estimated to be ca. –2.0 V vs. $(FeCp_2)^{+/0}$,[18] corresponding to an effective ionization energy (IE_{eff}) of 2.8 eV.[17] The energy-level diagram should be treated wth caution when comparing experimentally determined and DFT- derived quantities, given the uncertainties in estimating IE and EA from electrochemical potentials.[17] However, the energy diagram suggests $(RhCp^*Cp)_2$ can easily contribute electrons to the conduction bands of all four TMDs, whereas

electron transfer from the valence bands, especially those of the two disulfides, to the MB cation is of more marginal energetic feasibility.

We first demonstrate the effectiveness of the molecular dopants on atomically thin TMDs using electrical characterization of FETs. The characteristics of MoS_2, $MoSe_2$, WS_2, and WSe_2 FETs were measured before and after the molecular doping treatment. For the molecular doping treatment, FET devices were immersed in the dopant solutions of varied concentrations for various treatment times, rinsed with neat solvent several times followed by blow drying to remove any physisorbed unreacted dopants, while leaving dopant ions resulting from electron-transfer reactions in place. Electrical measurements were performed on top-contact, back-gated FETs made from monolayer MX_2 transferred onto a Si/SiO_2 substrate. Tens of devices were measured for each doping treatment (i.e., dopant concentration and treatment time). Figure 1(d-e) shows the schematics and optical microscopy image of a top-contact back-gated monolayer MX_2 FET. **Figure 2**a shows representative transport characteristics of a MoS_2 FET (with 10 nm Ti and 100 nm Au as the contact) before and after cumulative n-doping with $(RhCp^*Cp)_2$. The pristine MoS_2 FET displays n-type transport characteristics (Figure 2a, in black squares), as is often observed in the literature and which is attributable to sulfur vacancies.[19] A short 5 s dip into a dilute solution (0.25 mmol L^{-1}) clearly shifts the threshold voltage (V_{th}) of the transistor to a more negative gate voltage, which indicates n-doping. Also, both the on- and off-current increase by an order of magnitude. Then, the same sample was re-treated with a concentrated solution (2.5 mmol L^{-1}), and the current increased further, varying by less than one order of magnitude within the range of back-gate voltage (V_{bg}) examined (± 100 V); i.e., it exhibited a minimal on/off ratio, suggesting a high-level doping concentration (degenerate), in which the MoS_2 behaves as a near-metallic material. With an additional 10 min soaking in the 2.5 mmol L^{-1} n-dopant solution, the current did not significantly change for these values of V_{bg}, further supporting the likelihood of a degenerately n-doped MoS_2 channel. In contrast, degenerate n-doping of wafer-scale synthesized trilayer MoS_2 was not observed after prolonged

doping treatment in our previous studies,[11b] possibly due to different band structures and/or the quality of the MoS_2 films. To help demonstrate the effectiveness of MB as a p-dopant, a high work function metal Pd (10 nm) and Au 100 nm were used as the contacts. The p-doping treatments on MoS_2 devices with MB shifted the transfer curve to a more positive gate bias after a 10 s treatment with a solution of 5 mmol L^{-1} concentration (Figure 2b, blue circles).[20] After an additional 10 min and 1 h p-doping treatments on the same device, the V_{th} shifts to positive V_{bg} values, and an increase of about 2 orders of magnitude (compared to the pristine) in the hole current at negative gate voltage was observed. In this V_{bg} range, the MoS_2 device appears to be ambipolar with hole transport favored. p-Doped MoS_2 with low work-function metal (Ti/Au) electrodes has also been tested; however, a significant p-type (hole-transport) behavior of MoS_2 devices was not observed (Figure S3), presumably due to Fermi-level pinning of the Ti/Au contact metal close to the conduction band of MoS_2.[21] MoS_2 devices in the literature are mostly reported to show stubborn n-type behavior, even with high work-function metal contacts (e.g., Pd and Au) because of Fermi-level pinning at the interface,[19, 22] whereas other MX_2, such as WSe_2, have the Fermi level in the middle of the bandgap and no pinning occurs, making the modulation of polarity relatively easy.

As shown in Figures 2c-e, similar trends are observed for the other three MX_2 devices with n- and p-dopant treatments. In each case, two representative transport curves are shown in red for n-doping treatments, for dilute (0.25 mmol L^{-1}) and concentrated (2.5 mmol L^{-1}) solution treatments. Similarly, the p-doping treatments at higher concentration and longer time are shown as blue triangles. Both $MoSe_2$ and WS_2 appear to be degenerately n-doped after the second treatment (2.5 mmol L^{-1}, 1 s), but WSe_2 became degenerately doped only after the fourth 10 min treatment (overnight treatment was also tested, but with no obvious additional change observed). On the other hand, the transfer curves for WSe_2 exhibited stronger p-doping effects than those of the other three materials. Notably, degenerate doping was obtained after 1 h

treatment for this TMD, but was not observed for p-doped MoS_2, $MoSe_2$, and WS_2. Shifts in threshold voltage (ΔV_{th}) relative to the pristine sample (i.e.,. $\Delta V_{th,\ pristine} = 0$ V) are summarized in Figure 2f; tens of transistors were measured in each case to obtain the average ΔV_{th} and standard deviation represented by the error bars. At a high doping level, V_{th} became unmeasurable or out-of-range as indicated by a bar filling the entire range of V_{th} shifts of the relevant sign. For both the n- and p-doping side, the dark bars show the shorter treatment time (or lower concentration), and as the colors lighten, longer treatment time was performed. Overall, the extent of n-doping effects under a given set of conditions ($|\Delta V_{th,\ MoS_2}| > |\Delta V_{th,\ WS_2}| > |\Delta V_{th,\ MoSe_2}| > |\Delta V_{th,\ WSe_2}|$) is consistent with the positions of the DFT-calculated conduction band minima, and, thus, the ease of reduction of the four TMDs, and extent of p-doping ($|\Delta V_{th,\ MoS_2}| < |\Delta V_{th,\ WS_2}| < |\Delta V_{th,\ MoSe_2}| < |\Delta V_{th,\ WSe_2}|$), is consistent with the trends in valence-band maxima and, therefore, the ease of oxidation. The charge density, n, in MX_2 after doping was estimated based on the V_{th} shifts according to:

$$n = \frac{C_{bg}\Delta V_{th}}{e} \quad (1)$$

where $e = 1.6\times10^{-19}$, C is the electron charge, and $C_{bg} \approx 1.1\times10^{-8}$ F cm^{-2} is the back-gate capacitance estimated based on the parallel-plate capacitor model of 300 nm thick SiO_2. The 5 s dipping in 0.25 mmol L^{-1} n-dopant corresponds to increases of the electron density in the monolayer of (2.4×10^{12}, 1.7×10^{12}, 2.1×10^{12}, and 1.1×10^{12}) cm^{-2} for MoS_2, $MoSe_2$, WS_2, and WSe_2, respectively. The hole densities changes upon p-doping for 1 h are estimated to be 6.9×10^{12} cm^{-2}, 9.6×10^{12} cm^{-2}, and 7.5×10^{12} cm^{-2} for MoS_2, $MoSe_2$, and WS_2, respectively (no threshold voltage is observed at this doping level for WSe_2). The doping densities are comparable to previous reports.[11b,11c] To summarize the electrical measurements, the degenerate doping levels of all four materials (MoS_2, $MoSe_2$, WS_2, and WSe_2) have been achieved on the n-doping side, while only WSe_2 can be degenerately p-doped. This is consistent with their DFT-calculated band energies relative to the EA and IE levels of dopants shown in

Figure 1(b). The transport behavior of monolayer TMDs can be effectively controlled through the choice of dopant, solution concentration, and treatment time.

The PL properties of the four doped MX_2 monolayer samples were also characterized. **Figure 3a** shows the PL spectra of monolayer MoS_2 before (in black) and after n-doping (in red) or p-doping (in blue). Compared to the pristine MoS_2, PL intensity increases by a factor of two upon p-doping but decreases by a factor of three upon n-doping. Spatially resolved PL intensity maps of the MoS_2 flake show that the PL intensities are uniform across the 20 μm by 20 μm sized flake (Figure S4). Figure 3b shows the normalized MoS_2 PL spectra relative to the Si Raman peak at 521 cm^{-1} with peak fitting. The PL peak can be deconvoluted into two components attributed to the negatively charged trion (X^-) peak at ca. 1.85 eV and the neutral exciton (X) peak at ca. 1.89 eV.[23] Upon p-doping, the PL spectra are dominated by the exciton peak X; the trion weight of MoS_2, defined as $I_{x\text{-}}/I_{total}$, decreases gradually from 0.56 to 0.34 (Figure 3d) and the emission is overall blue-shifted. This is consistent with the decreasing number of the negative carriers, and therefore the formation of fewer trions trions as seen in the literature reports for MoS_2 films p-doped using F_4TCNQ.[23] n-Doping, however, suppresses the PL intensity for MoS_2. As shown in Figure 3(a-b), the exciton peak intensity decreases dramatically upon n-doping as the trion peak increases, as gauged by an increase in the trion weight from 0.56 to 0.67. Similar phenomena have been observed in the literature for gate-dependent MoS_2 PL spectra: at negative V_{bg} (p-doping), the overall PL intensity increases and the exciton peak becomes dominant; at positive V_{bg} (n-doping), the PL intensity decreases and the trion weight becomes a larger portion of the total intensity.[24] Following the work by Mouri et al. [23], we use the mass action law to relate the trion weight ($I_{x\text{-}}/I_{total}$) to the number of free carriers (see Supporting Information S4). The electron density for pristine monolayer MoS_2 is estimated to be 3.3×10^{13} cm^{-2}, decreases to 1.2×10^{13} cm^{-2} after 1 h p-doping, and increases to 5.1×10^{13} cm^{-2} after 1 h n-doping. The difference of electron density before and after 1 h p- and n-doping

treatment are evaluated as $\Delta n_{\text{p-dope}} = 2.1\times10^{13}$ cm^{-2} and $\Delta n_{\text{n-dope}} = 1.8\times10^{13}$ cm^{-2}, respectively. This value is about 3 times higher than the carrier density change calculated based on ΔV_{th} (n = 6.9×10^{12} cm^{-2}) for p-doped MoS_2.[25] This may be because the carrier density determined from PL depends on electrons populating excited states initiated by photoexcitation, which could be different from the contribution of free charge carriers to the drain current. The same trends were observed for all of the other three MX_2 materials: the PL intensity was enhanced upon p-doping and quenched upon n-doping. The PL spectra for all four MX_2 materials consists of both a dominant exciton peak at higher energy and a smaller trion peak at lower energy with a separation of approximately 0.03 eV to 0.04 eV, consistent with other reports[26]. The trion spectral weight ($I_{\text{x-}}/I_{\text{total}}$) decreases upon p-doping and increases upon n-doping. Here, we demonstrate that the PL for all the four MX_2 materials can be tuned effectively upon doping, but further experimental and theoretical studies are needed to fully understand this effect.

Raman spectroscopy was also performed to explore the doping effects on the phonons of the host MX_2. **Figures 4**a and 4b summarize the Raman spectra of monolayer MoS_2 before and after doping treatment, with the other three materials shown in the Figure S7. There are two important modes in the Raman spectra: the E^1_{2g} phonon mode is an in-plane vibration of both the metal and chalcogen atoms, while the A_{1g} peak is the out-of-plane vibration of just the chalcogen atoms. The peak positions as a function of doping for these two vibrational modes of MoS_2 are plotted in Figure 4b. For MoS_2, and for the other three MX_2 materials (Figure S7), n-doping leads to the red-shifting (to lower energy) for both vibrational modes, whereas p-doping leads to the blue-shift (to higher energy) for both modes.[27] This is consistent with previous studies, which observed that higher electron concentration in the n-doped film increases electron-phonon scattering,[28] whereas p-doping reduces the electron-phonon scattering with previously reported effects of doping for MoS_2 and WSe_2.[9a] As shown in Figure 4b, the higher sensitvitiy of the A_{1g} is due to the fact that the mode couples much more strongly

with electrons than the E_{2g} mode does.[27, 29] The Raman shift of A_{1g} mode on the n- doping side is larger than the p-doping side. This also confirmed that p-doping is less efficient than the n-doping for MoS_2 evidenced by their relative band energy levels. As compared with the Raman shifts observed in the literature,[27] we estimate the changes of carrier density are on the order of 10^{12} cm^{-2} for both n- and p-doped MoS_2, which is consistent with the charge sheet density calculated based on ΔV_{th}.

XPS was also performed to investigate the impact of doping on the MX_2 chemical structure and energy levels, specifically to characterize the 2.5 mmol L^{-1} 10 min n-doped MX_2 flakes and 5 mmol L^{-1} 1 h p-doped MX_2 flakes. Figure 4c shows the XPS core-levels of the main Mo 3d and S 2p for MoS_2 flakes. The spectral shape of the Mo and S photoemission lines after n- (in red) and p-doping (in blue) are nearly identical to that of the pristine material (in black), which indicates that the doping treatment does not significantly chemically alter the MoS_2 host. However, upon p-doping treatment, the core levels associated with the MX_2 shift to lower binding energy consistent with the Fermi level moving closer to the valence band maximum (i.e., occupied density of states), as expected. For all four MX_2 materials, p-doping leads to about 0.2 eV shifts to lower binding energy; i.e., E_F shifts closer to the E_V by ca. 0.2 eV. On the contrary, n-doping for MX_2 materials leads to the core-level peaks shifting toward higher binding energy by 0.2 eV to 0.3 eV, as the Fermi level is shifted away from the occupied density of states (i.e., valence band). The effect of molecular doping on the electronic structure of MX_2 is illustrated in Figure 4d: upon n-doping, the valence band maximum shifts away from the Fermi energy, and the X^- dominates the PL before finally being quenched. Conversely, when exposed to the p-dopant MB, the TMD valence band shifts closer to the Fermi energy, the X dominates the PL, and the PL intensity increases.

The coverage of absorbed doping product (cation or anion) was also estimated from the XPS data. In the case of p-doping, relatively strong Sb 3d and Cl 2p ionizations were observed,

consistent with the presence of $SbCl_6^-$ ions, while no detectable Br 3d features were seen (Figure S9), consistent with expectations that the neutral $N(C_6H_4\text{-}p\text{-}Br)_3$ molecules formed during the electron transfer from the MX_2 would be washed away in the rinsing step. Meanwhile, Rh 3d was detected on the n-doped films, the peak position being consistent with Rh(III) from the monomeric $[RhCp^*Cp]^+$, as observed in a previous study.[11c] The dopant:MX_2 ratio is estimated by comparing the peak intensity ratio of elements from the doping product to host MX_2 film and, given the MX_2 unit cell area (ca. 0.0843 nm^2 for single-layer MoS_2 and WS_2; ca. 0.0932 nm^2 for $MoSe_2$ and WSe_2) can be converted to a number of dopant ions and, therefore, number of electrons or holes contributed, per unit area. Furthermore, assuming the unit cell of a close-packed array of $SbCl_6^-$ ions has an area of 60.2 $Å^2$, and an array of close-packed $[RhCp^*Cp]^+$ ions orientated with their five-fold axes perpendicular to the surface would have a unit-cell area of 73 $Å^2$,[11a] the coverage can also be expressed as a percentage of an ideal dopant-ion monolayer, as described in previous reports.[11b, 11c] For MoS_2, a coverage of 42 % of a molecular monolayer was obtained after 1 h p-doping, and the change of hole sheet density induced by p-doping was estimated as 7.0×10^{13} cm^{-2}; the 10 min n-doping led to a higher desnsity, estimated as 8.9×10^{13} cm^{-2}. The change in carrier sheet density estimated from the XPS is three times the carrier density calculated based on the trion spectral weight from PL and 10 times higher than the charge sheet density calculated based on ΔV_{th}.[30] The fact that transport, PL, and XPS measurements agree within an order of magnitude is quite remarkable considering each has inherent assumptions and probes a different aspect of the doping interaction. In principle the XPS discrepancy arises if not all the dopants present on the surface had fully reacted and the charge-transfer efficiency was less than 100 %. Previous studies on graphene doping showed that the doping efficiency for this rhodium-based dimer can be as low as 50 %; however, the unreacted Rh(I) dimer could clearly distinguished from the Rh(III) cation in XPS spectra.[11a] Similarly, as noted above, only the $SbCl_6^-$ anions are detected in XPS of p-doped samples, also suggesting each dopant-derived ion does reflect contribution of a integral charge

tot he MX_2 layer. An alternative explanation is that some of the charge carriers transferred from the dopant may be trapped, for example by impurities and defects, or by strong electrostatic interactions with dopant ions, and therefore may not contribute to the PL change and drain current. The same methods were used to estimate the percentage monolayers and the numbers of charges transferred to the other doped films and, as summarized in Table S1, similar orders of magnitude were obtained.

In summary, we demonstrate a readily controllable, electron-transfer doping methodology for a series of monolayer group 6 disulfides and diselenides with a wide range of energy levels and of electrical and optical properties. Strong n- and p-doping effects were confirmed by transistor measurements, and by PL, Raman, and XPS spectroscopy. The transport behavior of all four TMDs can be controlled over a large range, including both non-degenerate and degenerate regimes through the choice of dopant, solution concentration, and treatment time. Surprisingly, even MoS_2, a strong n-type semiconductor, can be tuned to yield high-performance, p-channel behavior. The magnitude of the n- and p-doping effects achievable on the four MX_2 is consistent with DFT-calculated band energies. We also demonstrated tunable PL properties of these four monolayer materials. The PL intensity is enhanced through p-doping and quenched upon n-doping, and the spectral weight of trion vs. exciton contributions decreases from n-doped to p-doped samples, consistent with the expected change in the carrier density. Characterization by Raman and XPS also provides insight on the underlying physical mechanism of the molecular reductants and oxidants on the monolayer TMDs materials. This electron-transfer doping approach provides a simple and effective route to tailor the electrical and optical properties of TMDs.

Supporting Information

Supporting Information is available from the Wiley Online Library or from the author.

Acknowledgements

S. Z. acknowledges support from the National Institute of Standards and Technology (NIST) Financial Assistance Award with Federal Award ID 70NANB16H228. The authors are thankful to Dr. David J. Gundlach and Dr. Emily G. Bittle for their assistance with the electrical measurements, Dr. Hsin-Yen Lee for his help with PL and Raman data analysis, and Erik M. Secula for his advice and help for revision.

Received: ((will be filled in by the editorial staff))
Revised: ((will be filled in by the editorial staff))
Published online: ((will be filled in by the editorial staff))

References

[1] Q. H. Wang, K. Kalantar-Zadeh, A. Kis, J. N. Coleman, M. S. Strano, *Nat. Nanotechnol.* **2012**, 7, 699.

[2] a) K. S. Novoselov, A. K. Geim, S. V. Morozov, D. Jiang, Y. Zhang, S. V. Dubonos, I. V. Grigorieva, A. A. Firsov, *Science* **2004**, 306, 666; b) K. F. Mak, J. Shan, *Nat. Photonics* **2016**, 10, 216; c) B. Radisavljevic, A. Kis, *Nat. Mater.* **2013**, 12, 815.

[3] Y. Zhao, K. Xu, F. Pan, C. Zhou, F. Zhou, Y. Chai, *Adv. Funct. Mater.* **2017**, 27, 1603484.

[4] a) Y. Gong, Z. Liu, A. R. Lupini, G. Shi, J. Lin, S. Najmaei, Z. Lin, A. L. Elías, A. Berkdemir, G. You, H. Terrones, M. Terrones, R. Vajtai, S. T. Pantelides, S. J. Pennycook, J. Lou, W. Zhou, P. M. Ajayan, *Nano Lett.* **2014**, 14, 442; b) X. Duan, C. Wang, Z. Fan, G. Hao, L. Kou, U. Halim, H. Li, X. Wu, Y. Wang, J. Jiang, A. Pan, Y. Huang, R. Yu, X. Duan, *Nano Lett.* **2016**, 16, 264.

[5] a) M. R. Laskar, D. N. Nath, L. Ma, E. W. Lee, C. H. Lee, T. Kent, Z. Yang, R. Mishra, M. A. Roldan, J.-C. Idrobo, *Appl. Phys. Lett.* **2014**, 104, 092104; b) K. Dolui, I. Rungger, C. D. Pemmaraju, S. Sanvito, *Phys. Rev. B* **2013**, 88, 075420.

[6] M. Ghorbani-Asl, S. Kretschmer, D. E. Spearot, A. V. Krasheninnikov, *2D Materials* **2017**, 4, 025078.

[7] a) Y. Liu, H. Nan, X. Wu, W. Pan, W. Wang, J. Bai, W. Zhao, L. Sun, X. Wang, Z. Ni, *ACS Nano* **2013**, 7, 4202; b) M. Chen, H. Nam, S. Wi, L. Ji, X. Ren, L. Bian, S. Lu, X. Liang, *Appl. Phys. Lett.* **2013**, 103, 142110.

[8] a) S. Tongay, J. Zhou, C. Ataca, J. Liu, J. S. Kang, T. S. Matthews, L. You, J. Li, J. C. Grossman, J. Wu, *Nano Lett.* **2013**, 13, 2831; b) B. Cho, M. G. Hahm, M. Choi, J. Yoon, A. R. Kim, Y.-J. Lee, S.-G. Park, J.-D. Kwon, C. S. Kim, M. Song, Y. Jeong, K.-S. Nam, S. Lee, T. J. Yoo, C. G. Kang, B. H. Lee, H. C. Ko, P. M. Ajayan, D.-H. Kim, *Sci. Rep.* **2015**, 5, 8052.

[9] a) D.-H. Kang, M.-S. Kim, J. Shim, J. Jeon, H.-Y. Park, W.-S. Jung, H.-Y. Yu, C.-H. Pang, S. Lee, J.-H. Park, *Adv. Funct. Mater.* **2015**, 25, 4219; b) Y. Du, H. Liu, A. T. Neal, M. Si, D. Y. Peide, *IEEE Electron Device Lett.* **2013**, 34, 1328.

[10] a) M. Amani, P. Taheri, R. Addou, G. H. Ahn, D. Kiriya, D.-H. Lien, J. W. Ager, R. M. Wallace, A. Javey, *Nano Lett.* **2016**, 16, 2786; b) X. Liu, D. Qu, J. Ryu, F. Ahmed, Z. Yang, D. Lee, W. J. Yoo, *Adv. Mater.* **2016**, 28, 2345.

[11] a) S. A. Paniagua, J. Baltazar, H. Sojoudi, S. K. Mohapatra, S. Zhang, C. L. Henderson, S. Graham, S. Barlow, S. R. Marder, *Mater. Horiz.* **2014**, 1, 111; b) A. Tarasov, S. Zhang, M. Y. Tsai, P. M. Campbell, S. Graham, S. Barlow, S. R. Marder, E. M. Vogel, *Adv. Mater.* **2015**, 27, 1175; c) M.-Y. Tsai, S. Zhang, P. M. Campbell, R. R. Dasari, X. Ba, A. Tarasov, S. Graham, S. Barlow, S. R. Marder, E. M. Vogel, *Chem. Mater.* **2017**, 29, 7296.

[12] S. B. Desai, S. R. Madhvapathy, M. Amani, D. Kiriya, M. Hettick, M. Tosun, Y. Zhou, M. Dubey, J. W. Ager, D. Chrzan, A. Javey, *Adv. Mater.* **2016**, 28, 4053.

[13] O. V. Gusev, L. I. Denisovich, M. G. Peterleitner, A. Z. Rubezhov, N. A. Ustynyuk, P. M. Maitlis, *J. Organomet. Chem.* **1993**, 452, 219.

[14] F. Bell, A. Ledwith, D. Sherrington, *J. Chem. Soc. (C)* **1969**, 2719.

[15] C. Gong, H. Zhang, W. Wang, L. Colombo, R. M. Wallace, K. Cho, *Appl. Phys. Lett.* **2013**, 103, 053513.

[16] N. G. Connelly, W. E. Geiger, *Chem. Rev.* **1996**, 96, 877.

[17] a) Estimated assuming EA = eE_{red} + x eV and IE_{eff} = $eE(D^+/0.5D_2)$ + x eV and using x = 4.8, which is frequently used in the literature (x = 5.1 eV is also widely used and gives similar, but somewhat larger, values of both EA and IE_{eff}); b) J. Sworakowski, J. Lipiński, K. Janus, *Org. Electron.* **2016**, 33, 300.

[18] a) S. K. Mohapatra, A. Fonari, C. Risko, K. Yesudas, K. Moudgil, J. H. Delcamp, T. V. Timofeeva, J.-L. Brédas, S. R. Marder, S. Barlow, *Chem. Eur. J.* **2014**, 20, 15385; b) K. Moudgil, M. A. Mann, C. Risko, L. A. Bottomley, S. R. Marder, S. Barlow, *Organometallics* **2015**, 34, 3706.

[19] S. Chuang, C. Battaglia, A. Azcatl, S. McDonnell, J. S. Kang, X. Yin, M. Tosun, R. Kapadia, H. Fang, R. M. Wallace, *Nano Lett.* **2014**, 14, 1337.

[20] The concentration of p-dopant is twice of the n-dopant because each p-dopant MB molecule can accept one electron from the host materials while n-dopant dimer can donate two electrons.

[21] S. Das, H.-Y. Chen, A. V. Penumatcha, J. Appenzeller, *Nano Lett.* **2012**, 13, 100.

[22] C. Kim, I. Moon, D. Lee, M. S. Choi, F. Ahmed, S. Nam, Y. Cho, H.-J. Shin, S. Park, W. J. Yoo, *ACS Nano* **2017**, 11, 1588.

[23] S. Mouri, Y. Miyauchi, K. Matsuda, *Nano Lett.* **2013**, 13, 5944.

[24] K. F. Mak, K. He, C. Lee, G. H. Lee, J. Hone, T. F. Heinz, J. Shan, *Nat. Mater.* **2013**, 12, 207.

[25] The carrier density change calculated based on ΔVth on n-doping side is unavailable, because the Vth has shifted out of measurement range under the same condition. .

[26] B. Liu, W. Zhao, Z. Ding, I. Verzhbitskiy, L. Li, J. Lu, J. Chen, G. Eda, K. P. Loh, *Adv. Mater.* **2016**, 28, 6457.

[27] B. Chakraborty, A. Bera, D. Muthu, S. Bhowmick, U. V. Waghmare, A. Sood, *Phys. Rev. B* **2012**, 85, 161403.

[28] J. D. Lin, C. Han, F. Wang, R. Wang, D. Xiang, S. Qin, X.-A. Zhang, L. Wang, H. Zhang, A. T. S. Wee, W. Chen, *ACS Nano* **2014**, 8, 5323.

[29] G. Kukucska, J. Koltai, *Phys. Status Solidi B* **2017**, 254.

[30] All four TMDs reached degenerate regimes after 10 min n-doping and lose all the on/off ratio. Thus, the electron sheet density cannot be calculated.

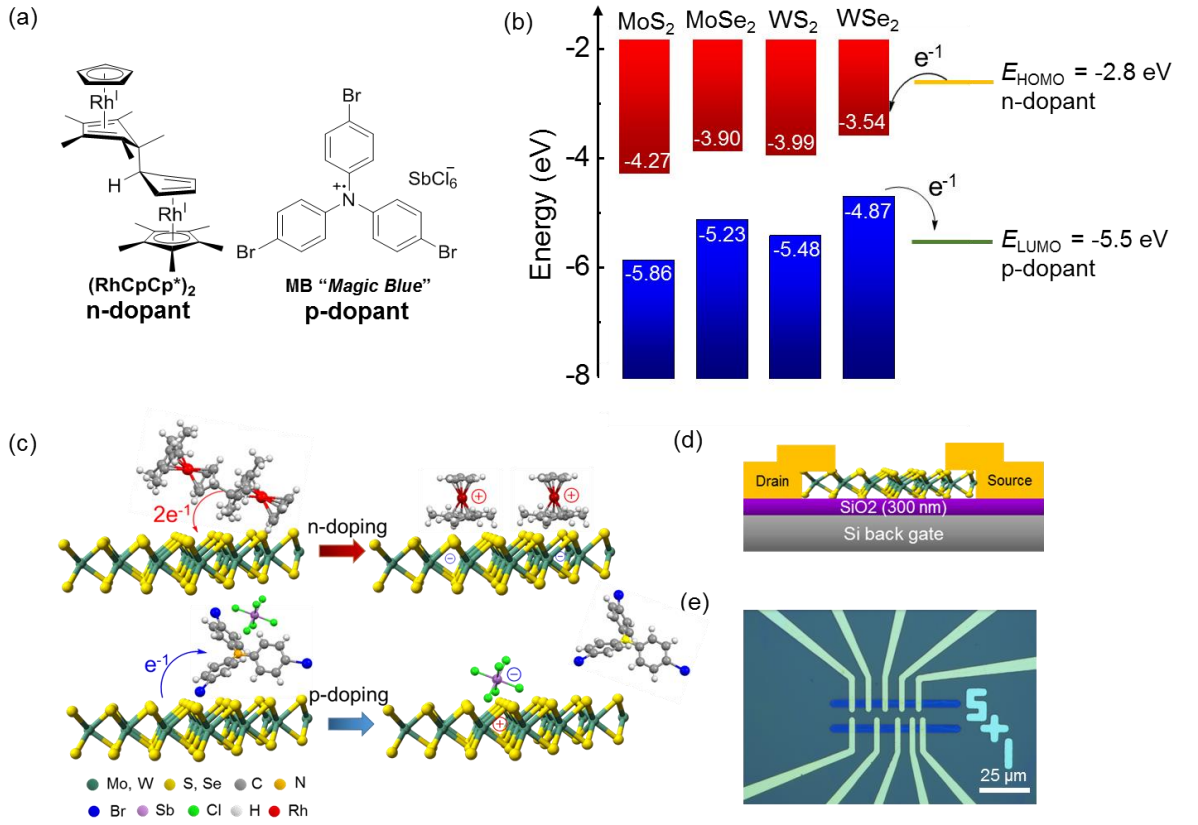

Figure 1. (a) Chemical structures of the molecular dopants used in this study. (b) Calculated band alignment of MoS_2, $MoSe_2$, WS_2, and WSe_2 from the literature[15] along with effective IE of the n-dopant and EA of the p-dopant estimated from electrochemistry. (c) Schematics of charge-transfer process for n- and p-doping. Monomeric RhCp*Cp is the expected product of n-doping. Treatment with MB is expected to form neutral tris(4-bromophenyl)amine and leave $SbCl_6^-$ anions on the surface. (d) Schematics of a top-contact back-gate monolayer MX_2 transistor. (e) Optical image of the MX_2 transistor.

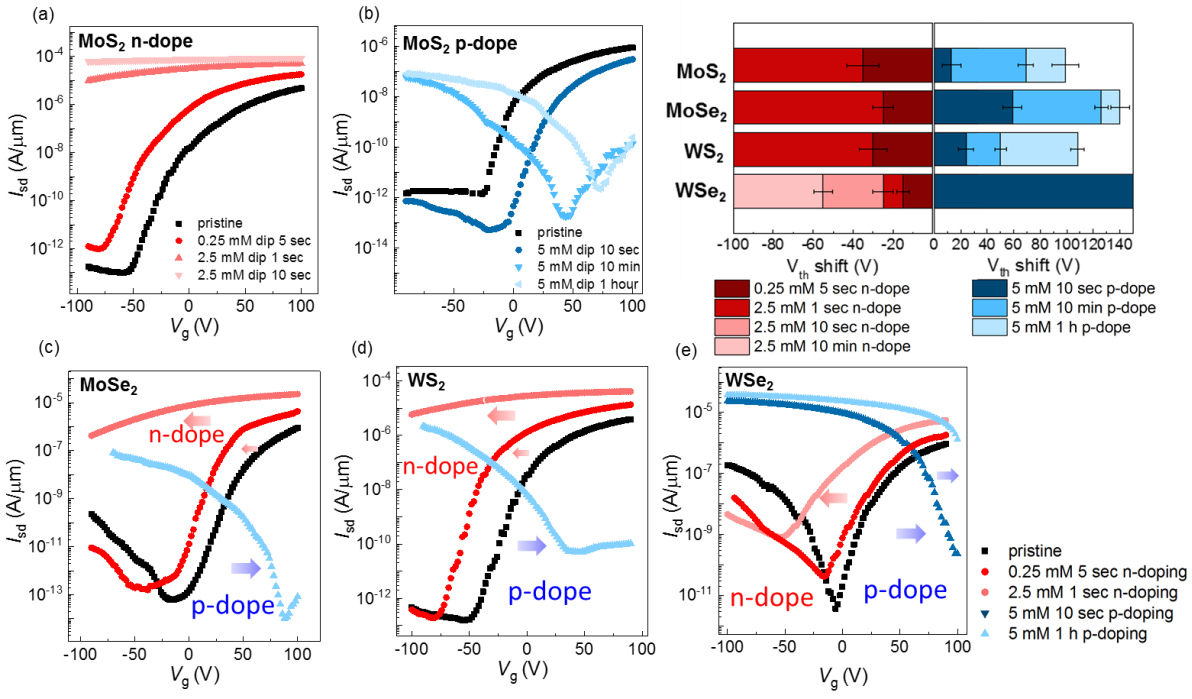

Figure 2. (a) Representative transfer characteristics of a pristine MoS_2 FET before any treatment and after continuously n-doping with $(RhCp^*Cp)_2$ with three different concentrations/exposure times. (b) Representative transfer characteristics of a pristine MoS_2 FET and after p-doping with MB for increasing exposure times with Pd/Au contact. (c-e) Representative transfer characteristics of the remaining three MX_2 FETs ($MoSe_2$, WS_2, and WSe_2) before and after doping with n- and p-dopants. Treating the transistor with n-dopant (red curve) shifts the threshold voltage V_{th} to more negative values, indicating n-doping (arrow). (f) Effects of different n- and p-dopant on the threshold voltage V_{th}. Threshold voltage shifts V_{th} shift are shown relative to the pristine sample (i.e., $V_{th,\ pristine} = 0$ V). Dark bars show the average V_{th} shift values after a short dip, whereas light bars represent longer treatment. Error bars indicate the standard deviation from averaging the results obtained with different devices.

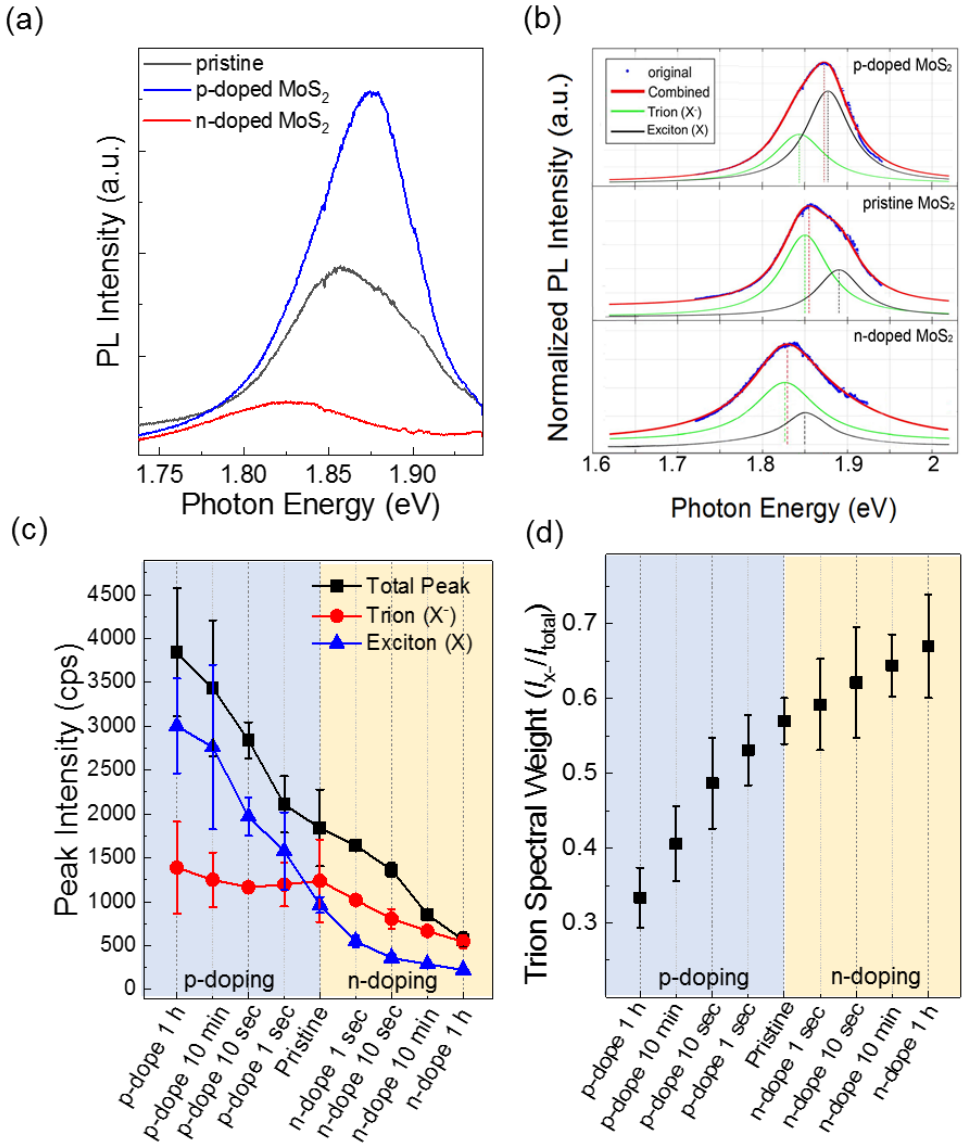

Figure 3. (a) PL spectra of MoS_2 after n- and p-doping treatment. (b) Analysis of the normalized MoS_2 PL spectra with the peak deconvolution. (c) The peak intensity of the two components and the sum of the MoS_2 PL spectra. (d) PL intensity weight of trion (I_{x^-}/I_{total}) as a function of the dopants treatment. Error bars indicate the standard deviation from averaging the results obtained with different spots.

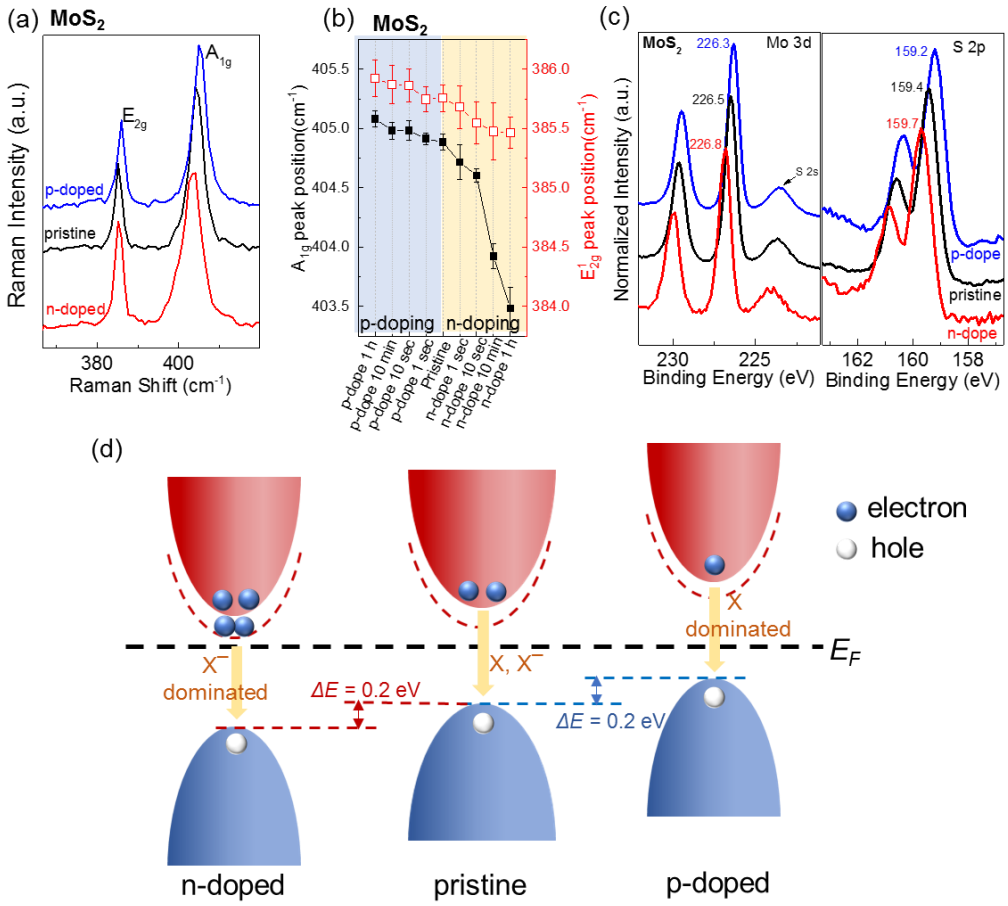

Figure 4. (a) Raman spectra of monolayer MoS_2 before and after different treatments with MB and $(RhCp^*Cp)_2$. (b) $E_{2g}{}^1$ and A_{1g} peak position shifts upon doping with different dopants. (c) XPS core-level Mo 3d and S 2p spectra for MoS_2 flake before and after dopant treatment. (d) Effects of molecular doping on the electronic structure of MX_2. Fermi levels are aligned. Error bars indicate the standard deviation from averaging the results obtained with different spots.

Supporting Information

Controllable, Wide-Ranging n- and p-Doping of Monolayer Group 6 Transition-metal Disulfides and Diselenides

Siyuan Zhang,[*] Heather M. Hill, Karttikay Moudgil, Curt A. Richter, Angela R. Hight Walker, Stephen Barlow, Seth R. Marder, Christina A. Hacker, Sujitra J. Pookpanratana**

Contents

1. General details

Bulk crystals of the four transition-metal dichalcogenides (TMDs) were purchased from HQ Graphene.[1] The monolayers were transferred according to the literature-reported gold-mediated exfoliation method.[2] All the MX_2 layers were transferred onto 300 nm thermally grown SiO_2 on a low-resistivity silicon wafer. The optical images, Raman and PL spectra were used to identify the number of layers. In this study, all the experiments were carried out on the monolayer MX_2, unless stated otherwise. The field effect transistors (FETs) were fabricated on the as-transferred monolayer MX_2 using the standard e-beam or photolithography method. Ti/Au or Pd/Au source-drain contacts were deposited through the e-beam evaporation followed by the lift-off process. The active area of the channel was patterned though a Unaxis 790 reactive ion etcher (RIE) using a mixture gas of SF_6 (45 sccm) and O_2 (5 sccm) at 100 W RF power for 20 s. Both the doping treatment and electrical measurements were carried out inside a Unilab MBraun glovebox under an atmosphere of nitrogen or argon with both water and oxygen level <0.5 ppm. The n-dopant, $(RhCp^*Cp)_2$ was synthesized according to the literature,[3] and p-dopant, tris(4-bromophenyl)ammoniumyl hexachloroantimonate ("Magic Blue," MB), was purchased from Sigma-Aldrich and used as received. $(RhCp^*Cp)_2$ was dissolved in anhydrous toluene to make a 2.5 mmol L^{-1} solution, and MB was dissolved in anhydrous DCM to make a 5 mmol L^{-1} solution. The concentration of p-dopant is twice the n-dopant, because each $(RhCp^*Cp)_2$ molecule is capable of supplying two electrons to the MX_2, while MB can only accept a single electron. All the transferred MX_2 samples were immersed in the dopant solutions for various treatment times and were then rinsed with fresh solvent three to five times to remove physisorbed dopants. The electrical characterization of the fabricated devices was collected using an Agilent 4155C Semiconductor Parameter Analyzer at room temperature inside an inert-atmosphere glovebox. A bottom-gate configuration was used with a 300 nm SiO_2 dielectric. The back-gate voltage V_{bg} is applied to the highly doped Si wafer (resistivity: 0.001 Ω cm to 0.01 Ω cm).

PL and Raman spectroscopy were acquired in a Renishaw InVia microscope spectrometer with laser excitation at 514 nm and 633 nm, and collected in backscattering configuration using a 50× objective. For all of the PL Raman measurements, the samples were transferred from the

glovebox using a sealed microscope stage to avoid air exposure during transfer and measurements steps. All PL and Raman peaks were calibrated based on the Si peak and fitted with Gaussian-Lorentzian line shapes to determine the peak position, the linewidth, and the intensity of different components. XPS Spectra were acquired on a Kratos Axis UltraDLD XPS/UPS system, under a base pressure of 10^{-9} Torr (10^{-7} Pa), using the monochromatic Al Kα line.

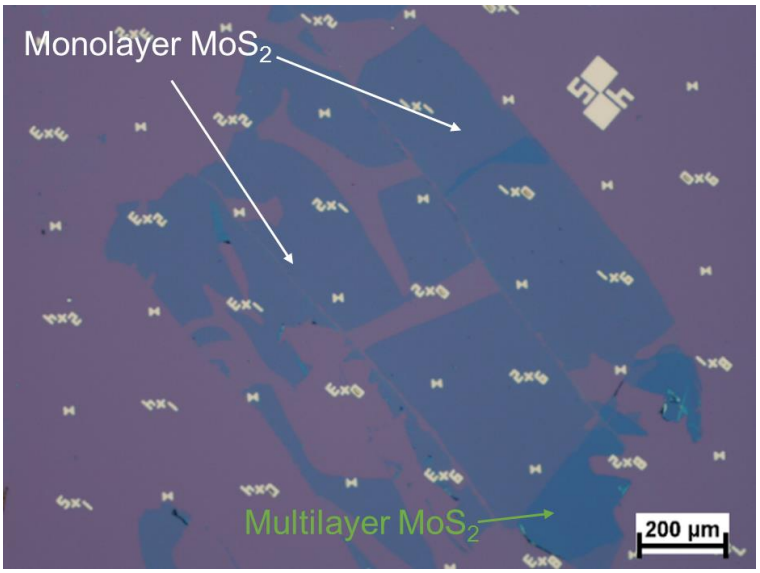

Figure S1. Optical images for the large-area gold-mediated exfoliated monolayer MoS_2.

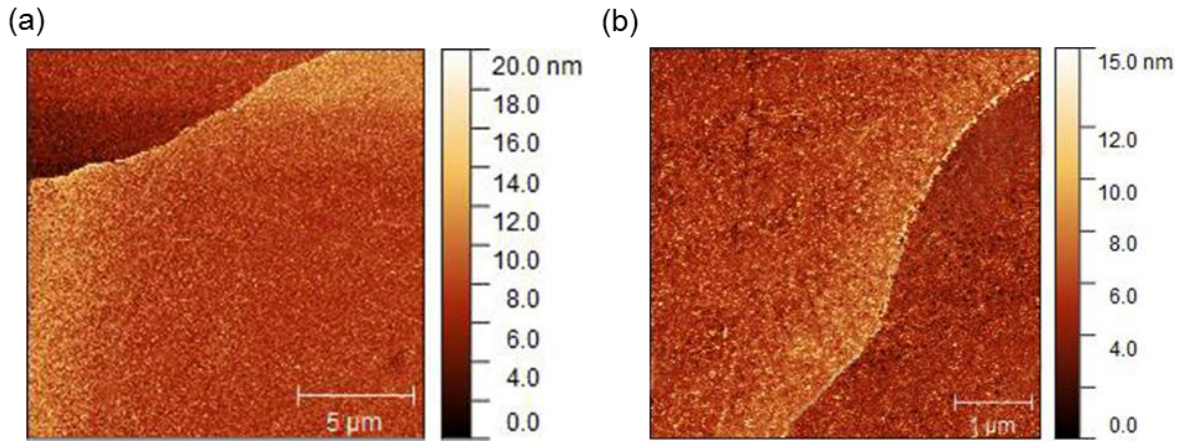

Figure S2. AFM images for the exfoliated monolayer MoS_2 (a) and $MoSe_2$ (b) as examples.

2. Additional FET results for MoS_2

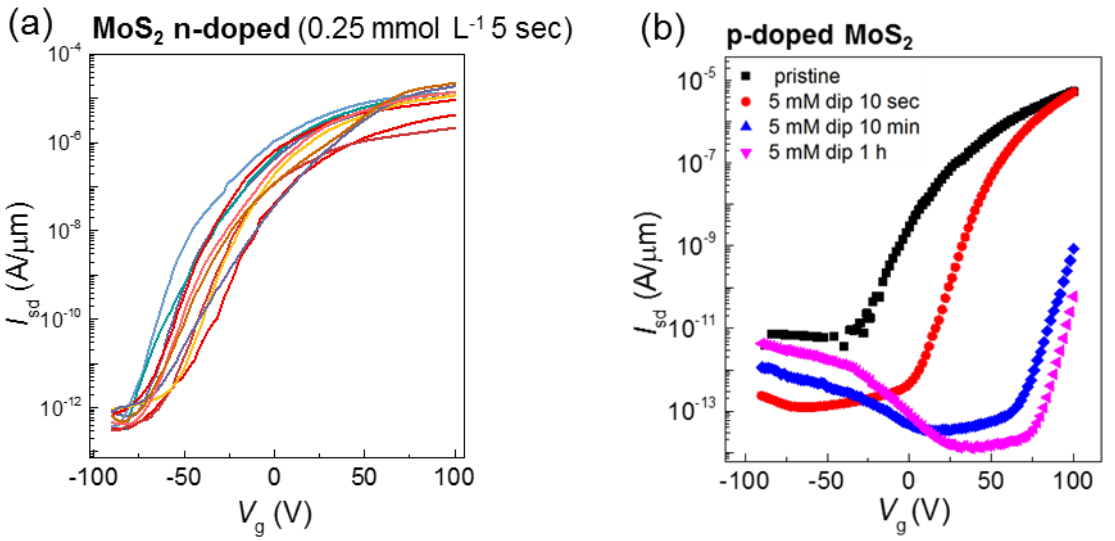

Figure S3. (a) Transfer characteristics of ten MoS_2 FETs after 5 sec treatment in 0.25 mmol L^{-1} solution showing the repeatability of the doping effect. (b) Representative transfer characteristics of a pristine MoS_2 FET after continuously p-doping with MB, using Ti/Au contacts.

3. Additional PL data

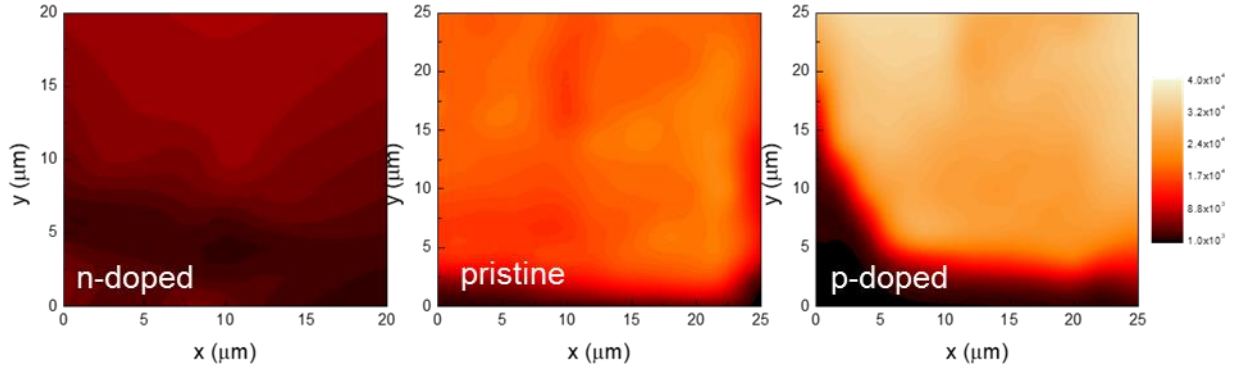

Figure S4. Spatially resolved PL intensity maps of the MoS_2 flake upon n- and p-doping. A strong PL signature at 1.86 eV is observed in the monolayer region of pristine MoS_2 (middle), while it is significantly quenched after n-doping (left) and the PL intensity is increased upon p-doping (right).

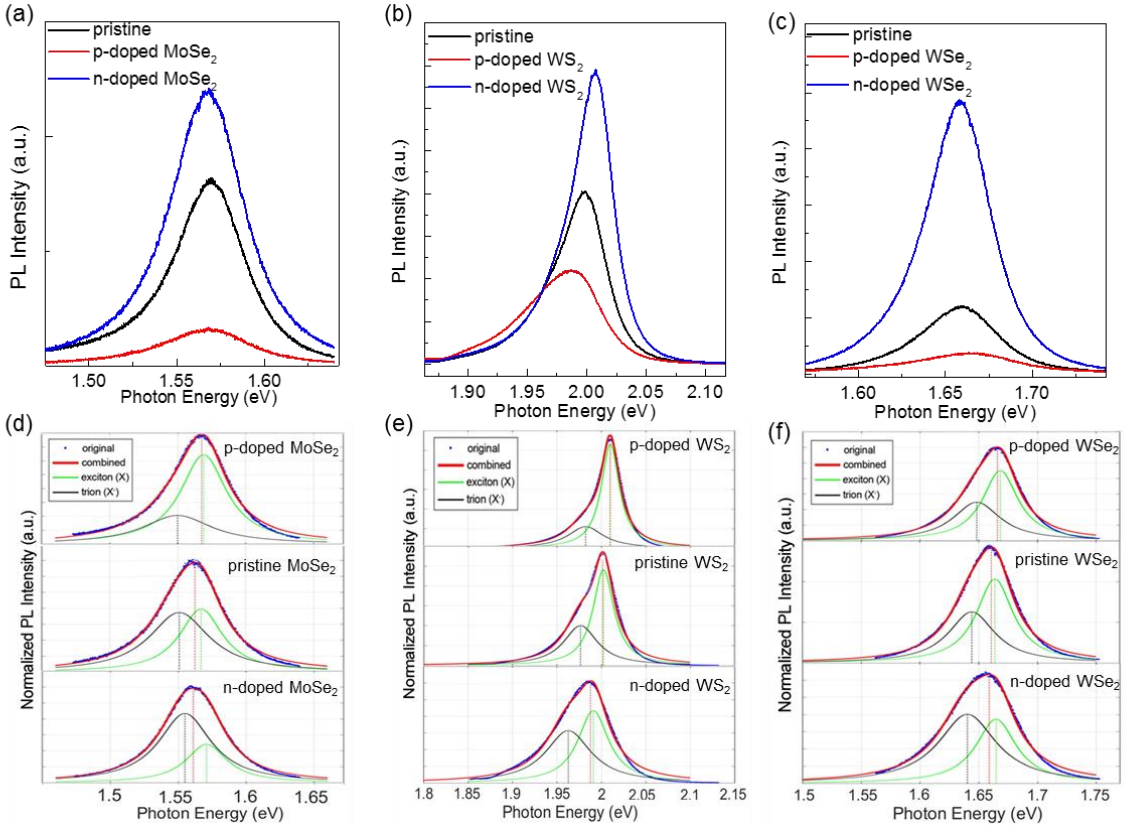

Figure S5. PL spectra of $MoSe_2$ (a), WS_2 (b) and WSe_2 (c) after n- and p-doping treatment. (b) Analysis of the normalized $MoSe_2$(d), WS_2 (e) and WSe_2 (f) PL spectra with the peak deconvolution.

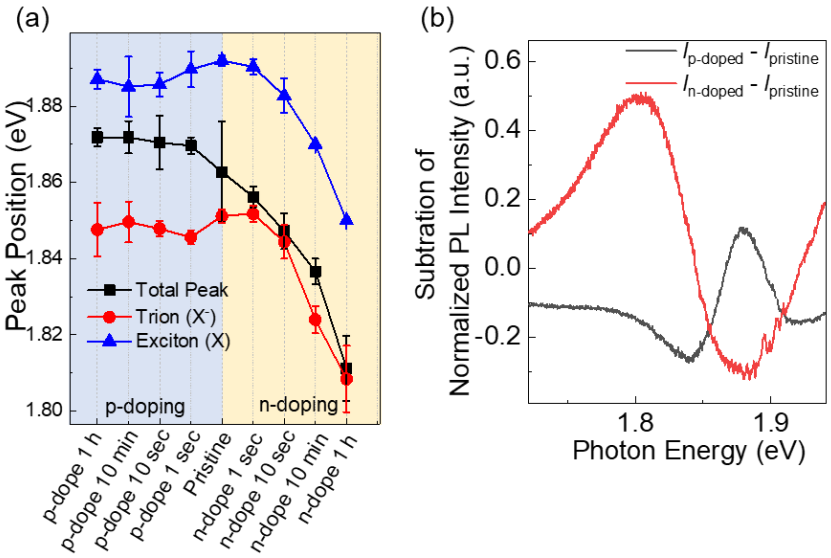

Figure S6. (a) The peak position shift for the two components and the sum of the MoS_2 PL spectra. (b) Subtraction of the normalized peak intensity for $I_{\text{p-doped}} - I_{\text{pristine}}$ (black curve) and $I_{\text{n-doped}} - I_{\text{pristine}}$ (red curve). Error bars indicate the standard deviation from averaging the results obtained with twenty different spots.

4. Estimation of the carrier density through mass action model

Following the work by Mouri et al. [4], we use the mass action law to relate the trion weight (I_{X^-}/I_{total}) to the number of free carriers. The trion weight (I_{X^-}/I_{total}) can be expressed as:

$$\frac{I_{X^-}}{I_{total}} = \left(\frac{\gamma_{tr}}{\gamma_{ex}}\frac{N_{X^-}}{N_X}\right) / \left(1 + \frac{\gamma_{tr}}{\gamma_{ex}}\frac{N_{X^-}}{N_X}\right) \approx \frac{4\times10^{-14} n_{el}}{1 + 4\times10^{-14} n_{el}} \quad (1)$$

where γ_{tr} and γ_{tr} are the radiative decay rates of trions and excitons, and N_X and N_{X^-} are the population of excitons and trions.[4] Replacing $\frac{N_{X^-}}{N_X}$ with the relation from the mass action law and using the exciton and trion radiative decay rates Mouri et al. extracted from fits to their data, we can write the trion weight as a function of the carrier density.

5. Additional Raman data for different MX_2

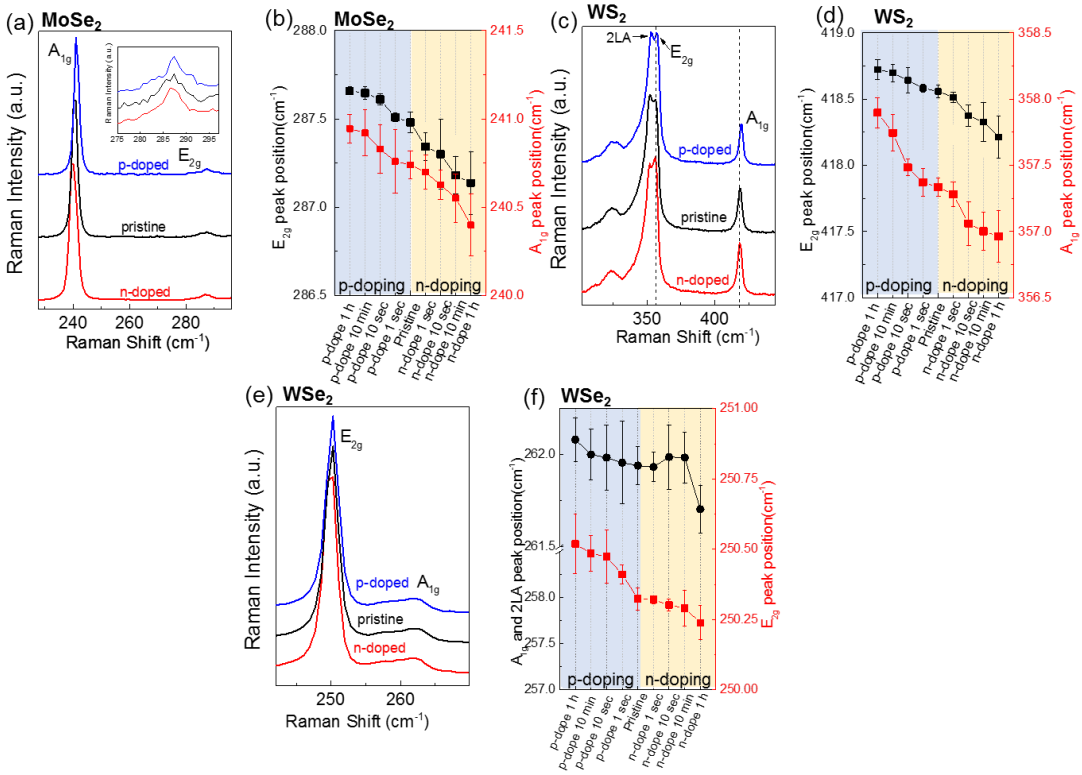

Figure S7. Raman spectra, and the E_{2g}^1 and A_{1g} peak position shifts upon doping with different dopants for monolayer $MoSe_2$ (a-b), WS_2 (c-d), and WSe_2 (e-f). Error bars indicate the standard deviation from averaging the results obtained with twenty different spots.

6. Additional XPS data for different MX_2 and calculations of surface coverage

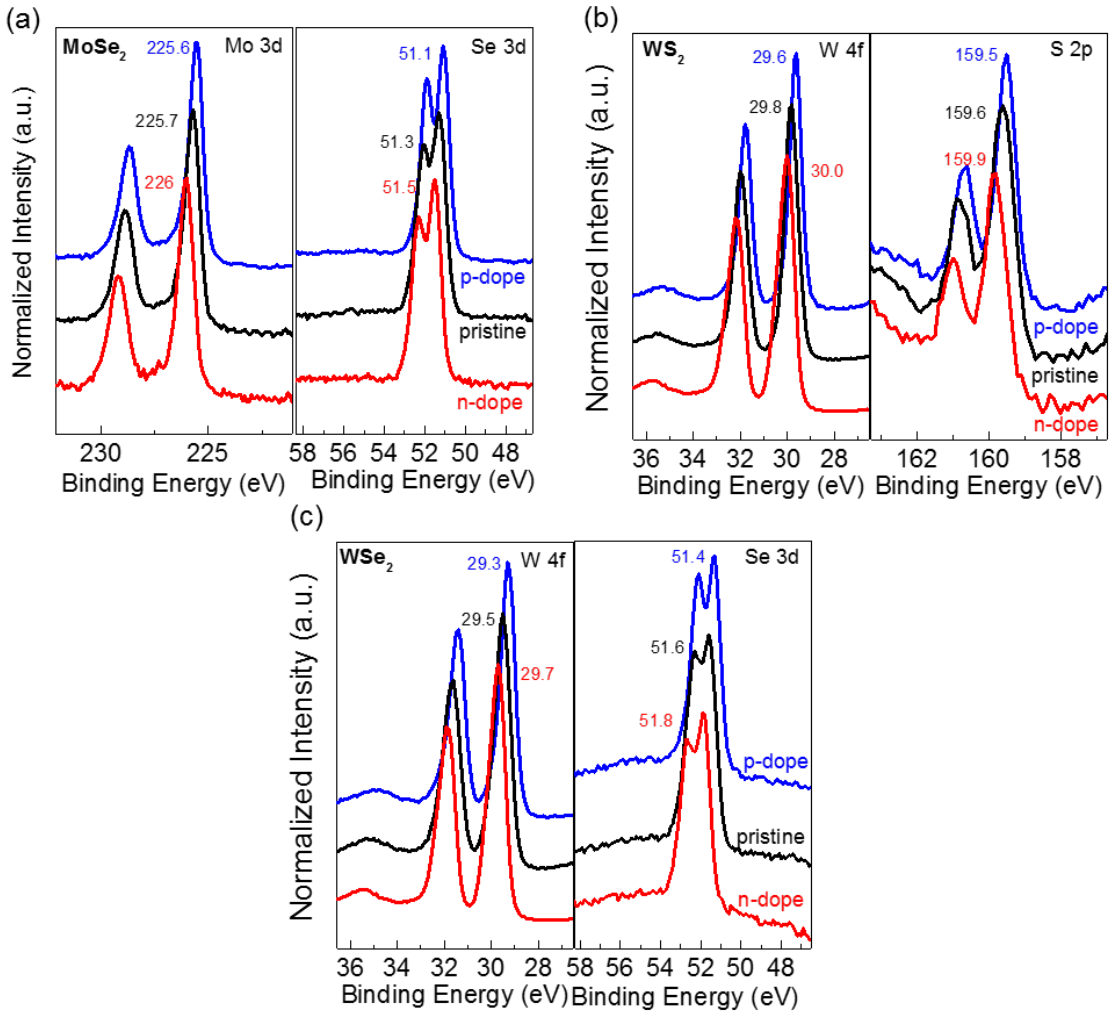

Figure S8. (a) The core-level Mo 3d and Se 3d spectra for $MoSe_2$ flake before and after dopant treatment. (b) XPS core-level W 4f and S 2p spectra for WS_2 flake before and after dopant treatment. (c) XPS core-level W 4f and Se 3d spectra for WSe_2 flake before and after dopant treatment.

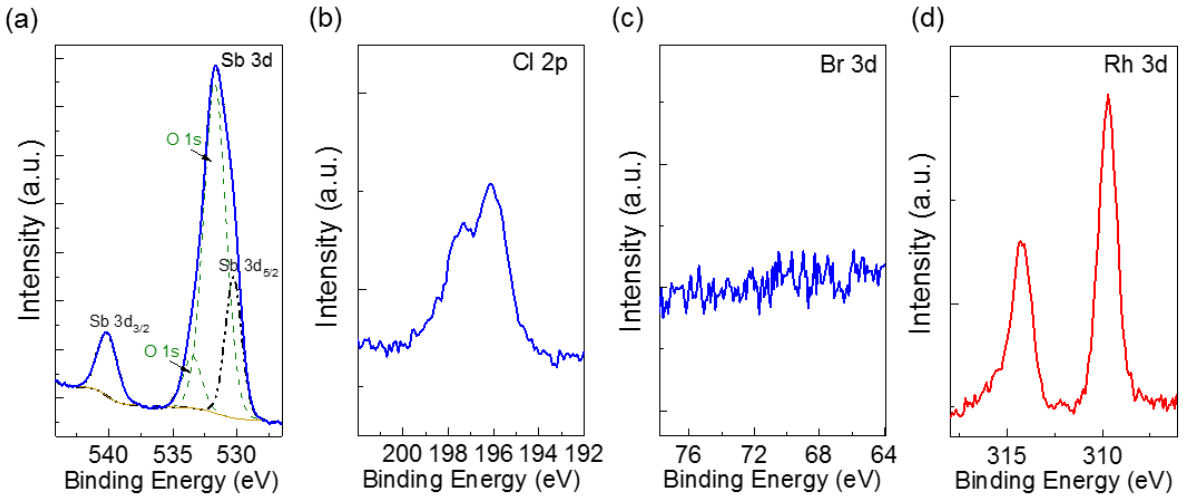

Figure S9. XPS core-level Sb 3d (a) and Cl 2p (b) from the anion of p-dopant MB, and Br 3d region (c), showing the absence of the cation of MB and of the corresponding neutral amine, on the p-doped MX_2 film. (d) Rh 3d from the n-doped film, attributable to the $(RhCp^*Cp)^+$ cation.

Table S1. Estimates of coverage (% of the close-packed monolayer) and the number of dopant ions on the surface of the monolayer MX_2.

Host Materials		MoS_2	$MoSe_2$	WS_2	WSe_2
p-doping	Elements	Sb 3d/Mo 3d	Sb 3d/Mo 3d	Sb 3d/W 4f	Sb 3d/W 4f
	Atomic Ratio	0.059 ± 0.013	0.074 ± 0.007	0.069 ± 0.006	0.087 ± 0.010
	% of close-packed ML	42 ± 8	48 ± 5	49 ± 4	56 ± 8
	No. of absorbed $(SbCl_6)^-$ anions /10^{13} cm^{-2}	7.0 ± 1.5	8.0 ± 0.8	8.2 ± 0.7	9.3 ± 1.3
n-doping	Elements	Rh 3d/Mo 3d	Rh 3d/Mo 3d	Rh 3d/W 4f	Rh 3d/W 4f
	Atomic Ratio	0.075 ± 0.008	0.070 ± 0.003	0.069 ± 0.005	0.057 ± 0.003
	% of close-packed ML	65±7	55±2	60±8	45 ± 3
	No. of absorbed $(RhCp^*Cp)^+$ cations/10^{13} cm^{-2}	8.9±1.2	7.5±0.5	8.2±1.1	6.2 ± 0.4

7. Electrical and PL Measurements of MX_2 Treated with Solvent

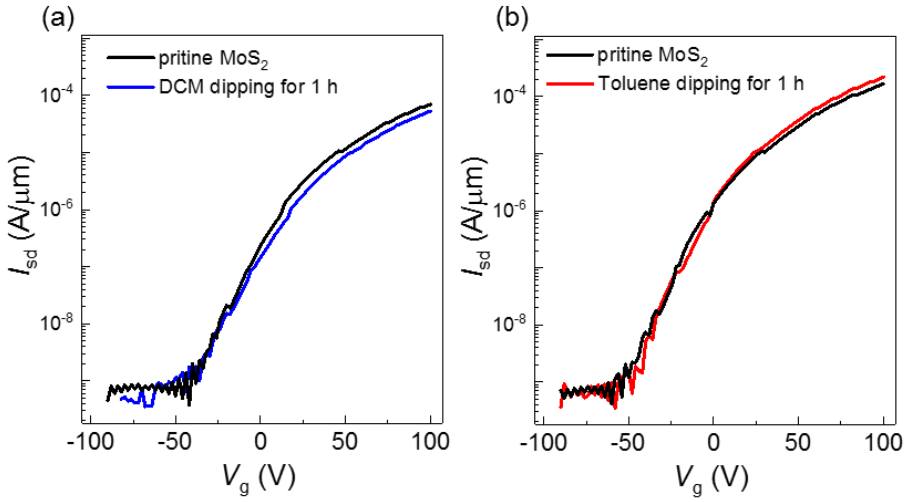

Figure S10. Transfer characteristics of a pristine MoS_2 FET before and after dipping into dichloromethane (DCM) (a) and toluene (b) for 1 h.

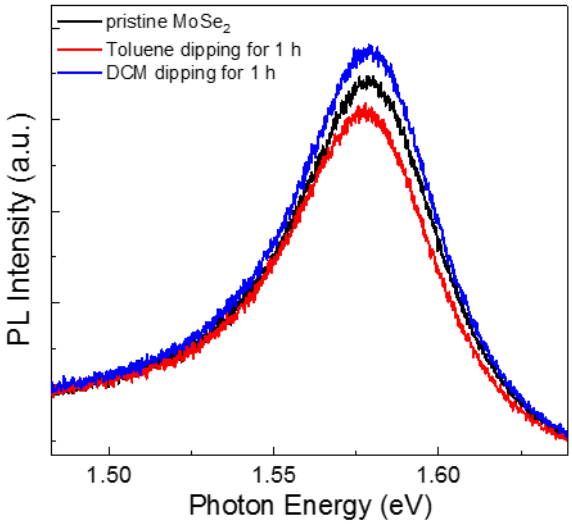

Figure S11. PL spectra of monolayer $MoSe_2$ before and after immersion in toluene and dichloromethane (DCM) for 1 h.

8. Air Stability Test of the Dopants

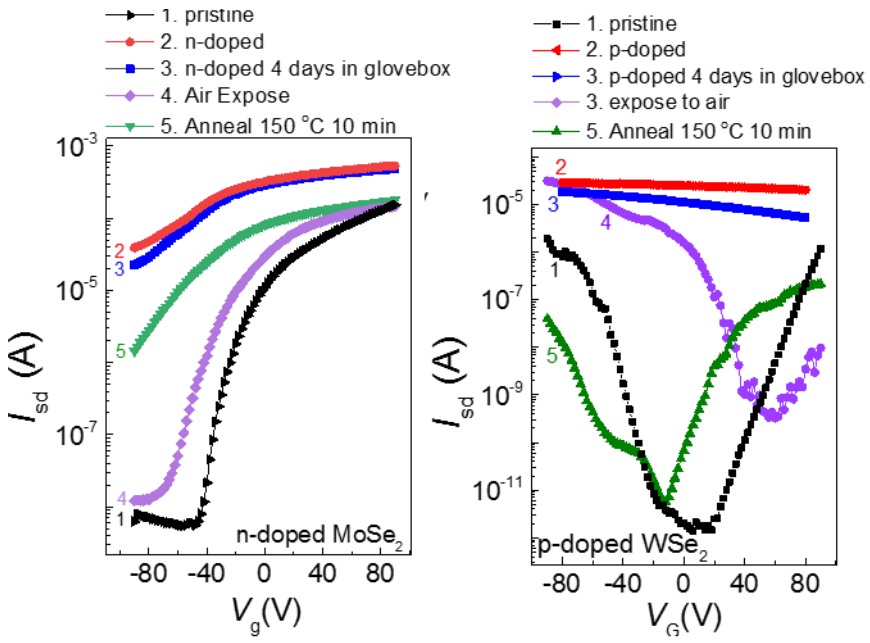

Figure S11. Stability test for the representative I_{sd}-V_g curves of n-doped $MoSe_2$ and p-doped WSe_2.

9. References

[1] All the commercial instruments and materials mentioned here are identified to foster understanding. Such identification does not imply recommendation or endorsement by the National Institute of Standards and Technology, nor does it imply that the materials or equipment identified are necessarily the best available for the purpose.

[2] S. B. Desai, S. R. Madhvapathy, M. Amani, D. Kiriya, M. Hettick, M. Tosun, Y. Zhou, M. Dubey, J. W. Ager, D. Chrzan, A. Javey, *Adv. Mater.* **2016**, 28, 4053.

[3] a) O. V. Gusev, L. I. Denisovich, M. G. Peterleitner, A. Z. Rubezhov, N. A. Ustynyuk, P. M. Maitlis, *J. Organomet. Chem.* **1993**, 452, 219; b) S. Guo, S. K. Mohapatra, A. Romanov, T. V. Timofeeva, K. I. Hardcastle, K. Yesudas, C. Risko, J. L. Brédas, S. R. Marder, S. Barlow, *Chem. Eur. J.* **2012**, 18, 14760.

[4] S. Mouri, Y. Miyauchi, K. Matsuda, *Nano Lett.* **2013**, 13, 5944.